Boosting blister formation on EUV masks by hydrogen and water vapor

Naoki Hayase,[a] Hayato Ishida,[a] Wataru Nishida,[b] Keishi Tsukiyama,[b] Shinji Yamakawa,[a] Tetsuo Harada[a*]

[a] Center for EUV lithography, LASTI, University of Hyogo, 1-1-2 NewSUBARU synchrotron radiation facility, Ako-gun Kouto, Hyogo 678-1205, Japan

[b] AGC Inc. Yokohama Technical Center 1-1, Suehiro-cho, Tsurumi-ku, Yokohama-shi, Kanagawa 230-0045 Japan

Abstract: Blister formation on extreme ultraviolet (EUV) masks by EUV-induced plasma irradiation is a problem that causes patterning errors. We investigated the blister formation under EUV-induced plasma containing hydrogen and water vapor through an accelerated mask lifetime test. **Background:** Interaction between hydrogen gas and EUV radiation generates hydrogen ions and radicals which react with contaminants. Hydrogen gas is introduced as a background gas in EUV scanners to remove contaminants, but EUV-induced hydrogen plasma forms blisters on EUV masks. Accelerated mask lifetime tests have reported on EUV-induced hydrogen plasma durability but the effect of residual water vapor on blister formation remains unclear. **Aim:** We evaluate the impact of water vapor on blister formation through EUV accelerated mask lifetime tests at NewSUBARU synchrotron radiation facility. **Approach:** The EUV intensity was in the range of approximately 20 to 45 W/cm², and hydrogen pressure was varied from 5 to 70 Pa with and without water vapor at around 10^{-3} Pa. The hydrogen pressures were controlled, and the EUV exposure dose was determined from the blister formation time in accelerated mask lifetime tests. The surface oxidation of the irradiated positions on the EUV masks was investigated by X-ray absorption spectroscopy (XAS), Rutherford backscattering spectrometry (RBS), and hydrogen forward scattering spectrometry (HFS). **Results:** The test revealed the dependence of blister formation on hydrogen pressure, both with and without water vapor. We observed enhanced blister formation and greater surface oxidation while applying water vapor, compared to introducing hydrogen alone on EUV masks. **Conclusion:** We clarify that the residual water vapor significantly affects the EUV dose and hydrogen pressure thresholds for blister formation under scanner-relevant conditions. The result provides insight into plasma-induced oxidation and contributes to mask process development.

Keywords: EUV; EUV-induced plasma; hydrogen; water vapor; mask blank; photomask.

E-mail: hayase@lasti.u-hyogo.ac.jp

1 Introduction

Extreme ultraviolet (EUV) lithography has been adopted for high-volume manufacturing at the 7 nm node process and beyond [1]. EUV scanners introduce hydrogen as background gas in order

to maintain the cleanliness of the inner walls, mirrors, and photomasks [2-5]. EUV light ionizes and dissociates hydrogen to generate plasma, which causes layer delamination on EUV masks, known as “blister” in Fig. 1 [6-10]. To investigate the blister formation process, EUV accelerated lifetime testing tools with hydrogen gas have been developed to reproduce EUV lithography in a shorter time [11-17]. The relationship between blister formation and EUV-induced hydrogen plasma exposure conditions has been reported [18-22]. Furthermore, it is important to consider how residual water vapor modifies surface oxidation to reproduce scanner-relevant blistering.

EUV irradiation of surfaces leads to photoemission of electrons and secondary electron generation [23-25]. The internal electric field across the oxide drives oxygen ions toward the oxide–metal interface, promoting oxidation at temperatures where thermal diffusion alone is negligible, and modifies interfacial bonding and the mechanical state of the layers. EUV-induced hydrogen plasma supplies low-energy ions and highly reactive radicals. Hydrogen can be taken up by near-surface layers, diffuse beneath coatings, and accumulate at interfaces. This uptake changes the stress state of the coating and can contribute to pressurization and interfacial debonding. Blister formation has been reported to be significantly severe in EUV-irradiated regions (the yellow dashed circle in Fig. 1), which is attributed to bond weakening in layers by secondary electrons that lowers chemical barriers [26-29]. This indicates that EUV-induced oxidation by hydrogen and water vapor degrades film adhesion, leading to blister formation [30].

In this paper, we investigated blister formation process on EUV masks exposed to hydrogen and water vapor. Our measurement evaluated the dependences of the pressure and EUV intensity via the accelerated lifetime tests at NewSUBARU synchrotron radiation facility.

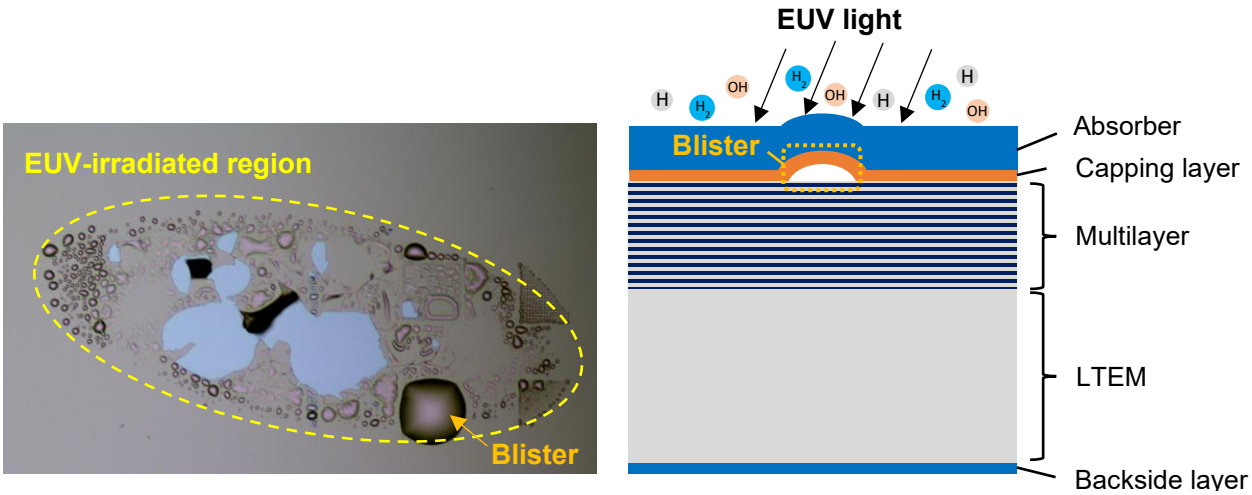

Fig. 1 (a) Image of blister on EUV mask surface (Ref [10]), (b) Schematic of blister on EUV masks.

2 Equipment

2.1 Accelerated mask lifetime test

Fig. 2-(a) shows the beamline 9C (BL9C) at NewSUBARU synchrotron radiation facility. BL9C provides hydrogen via a water electrolysis generator with a hydrogen purifier, and pure water in Fig. 2-(b) and (c). EUV intensity for the accelerated mask lifetime test is calculated by Eq. (1).

$$\phi_{\mathrm{EUV}} = \frac{I}{S} \times \frac{1}{a \times b} \times \frac{1}{\tau} \tag{1}$$

where I is the beam current of photodiode, S is the measured sensor sensitivity, a and b are width and height of the beam spot, τ is the transmittance of the attenuation filter. In this study, we used a photodiode with S of 0.102 A/W, τ is 1/40, and the beam size of a and b are approximately 0.8 mm and 0.3 mm, respectively. A YAG scintillator and a visible camera were used to image the beam spot size, as shown in Fig. 2-(d) and 2-(e), and measured the beam current by the photodiode. The cumulative dose for blister formation can be derived by the integration of the measured intensity by the blister formation time as Eq. (2).

$$Dose = \int_0^{t_{blister}} \phi_{\mathrm{accl}} dt \tag{2}$$

where ϕ_{accl} is the EUV intensity of accelerated exposure test, $t_{blister}$ is the blister formation time.

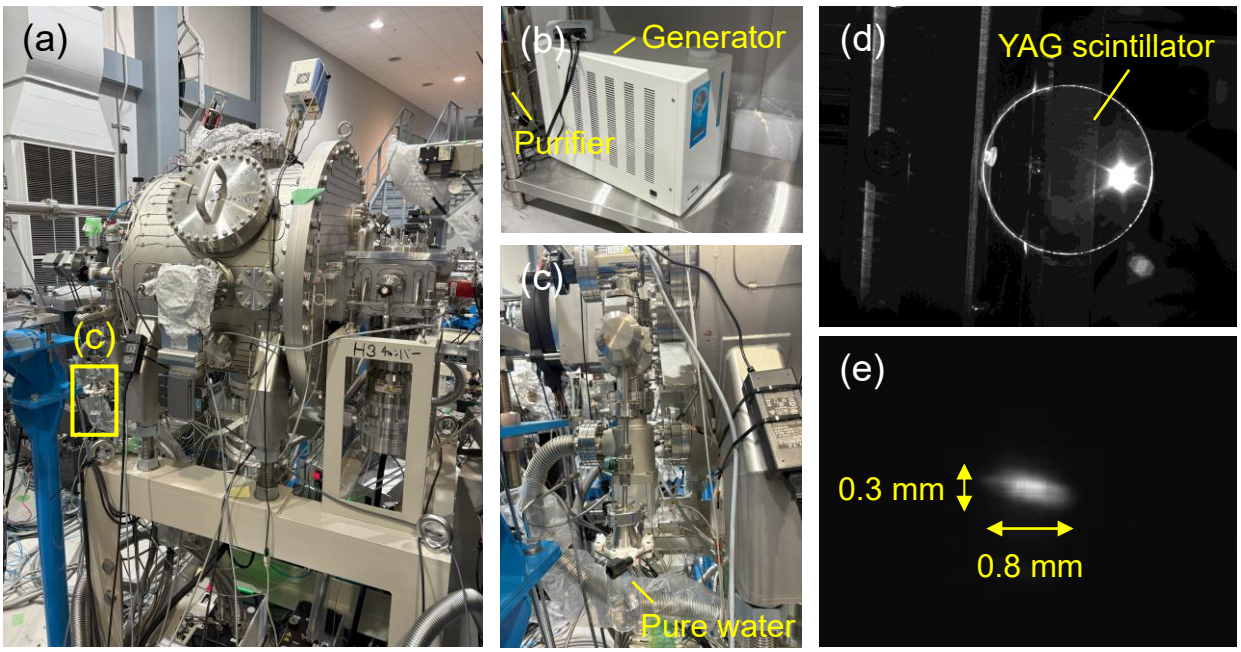

Fig. 2 (a) Overview of BL9C at NewSUBARU synchrotron radiation facility, (b) The electrolysis hydrogen generator with purifier, (c) The pure water supplier, (d) YAG scintillator, (e) The EUV beam spot.

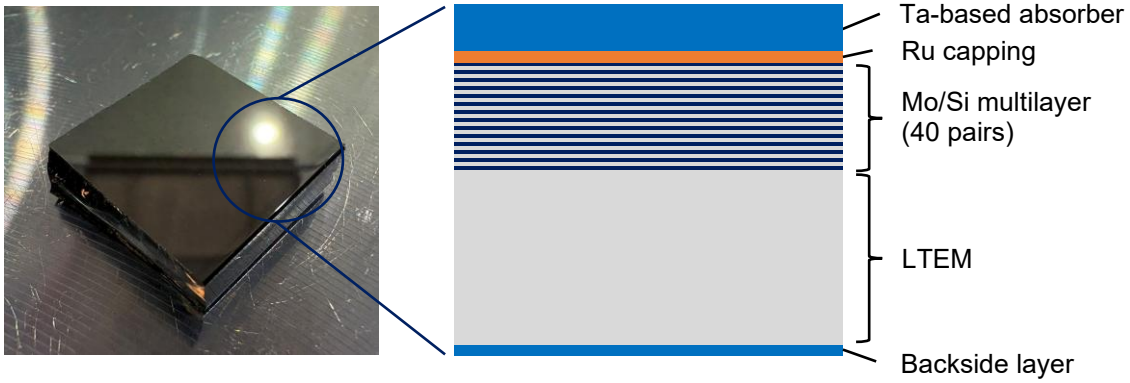

Fig. 3 The image of EUV mask blank fragment (20 mm × 20 mm) and the schematic of EUV mask blank.

2.2 Mask blanks and Photomasks

Fig. 3 shows the EUV mask blank fragments provided by AGC. The mask blanks are configured with Mo/Si multilayer (ML) of 40 pairs, Ru capping layer, and Ta-based absorber on a low thermal expansion material (LTEM) substrate. We used two types of mask blanks fabricated by different processes: Sample A, in which the film adhesion was deliberately weakened, and Sample B, which was fabricated according to the standard process. We also prepared the EUV photomask fragments, based on the non-AGC mask blanks. The photomask structures were the same as Fig. 3, but materials and processes were different.

3 Blister formation

3.1 Mask blanks

Table 1 shows the EUV-accelerated lifetime test results for mask blank and photomask fragments #1 to #9. #1 to #4 were measured at hydrogen pressures of 70, 30, 15, and 5 Pa at an EUV intensity of around 35 W/cm². Blisters were observed at 70, 30, and 15 Pa after 110, 165, and 230 minutes, corresponding to onset doses of 229.6, 344.4, and 500.0 kJ/cm², respectively, while no blister was observed at 5 Pa over 8 hours of irradiation. #5 was irradiated at 21.1 W/cm² and 70 Pa, with blister formation at 192 minutes corresponding to a total dose of 242.8 kJ/cm², a 5.4% difference from #1.

#6 to #8 were measured under hydrogen and water vapor, and the water vapor pressure was constant at 10^{-3} Pa. Blisters were observed after 95 minutes at 70 Pa (#6), 95 minutes at 30 Pa (#7),

and 290 minutes at 5 Pa (#8), corresponding to blister formation doses of 206.5 kJ/cm², 206.5 kJ/cm², and 622.1 kJ/cm², respectively. Sample B (#9) was irradiated through 385 minutes at 42.7 W/cm² under hydrogen pressure of 70 Pa and the water vapor pressure of 10^{-3} Pa. No blister formation was observed on Sample B (#9) up to the dose of 986.3 kJ/cm² which is more than four times the blister formation dose of Sample A (#6).

Fig. 4 shows the EUV exposure dose dependence of blister formation on hydrogen and water pressures, and blister formation dose decreases inversely with hydrogen pressure. The blister formation dose was 23.1 kJ/cm² lower for #6 than for #1, and 138.0 kJ/cm² lower for #7 than for #2. The impact of water vapor on blister formation became more significant at lower hydrogen pressures, with the greatest difference observed between #8 and #4.

Fig. 5 shows the microscope images of blisters and film delamination. In #1 and #2, the circular layer delamination was confirmed at five locations, with one blister also observed. The blisters and delamination areas had diameters of approximately 50 μm in all cases. #3 shows one blister of approximately 100 μm. In the cases of hydrogen and water vapor introduction, larger blisters of about 400 μm were observed in #6 and #8. Delamination was also observed in #7, following the appearance of film floating.

Table 1 Hydrogen and water vapor plasma durability test results on EUV mask blanks

No.	Sample	EUV intensity (W/cm^2)	H_2 Pressure (Pa)	H_2O Pressure (Pa)	Blister	Blister formation time (min)	Blister formation dose (kJ/cm^2)
1	Sample A	34.8	70	0	**Observed**	110	229.6
2		34.8	30	0	**Observed**	165	344.4
3		36.2	15	0	**Observed**	230	500.0
4		35.9	5	0	None		
5		21.1	70	0	**Observed**	192	242.8
6		36.2	70	10^{-3}	**Observed**	95	206.5
7		36.2	30	10^{-3}	**Observed**	95	206.5
8		35.8	5	10^{-3}	**Observed**	290	622.1
9	Sample B	42.7	70	10^{-3}	None		

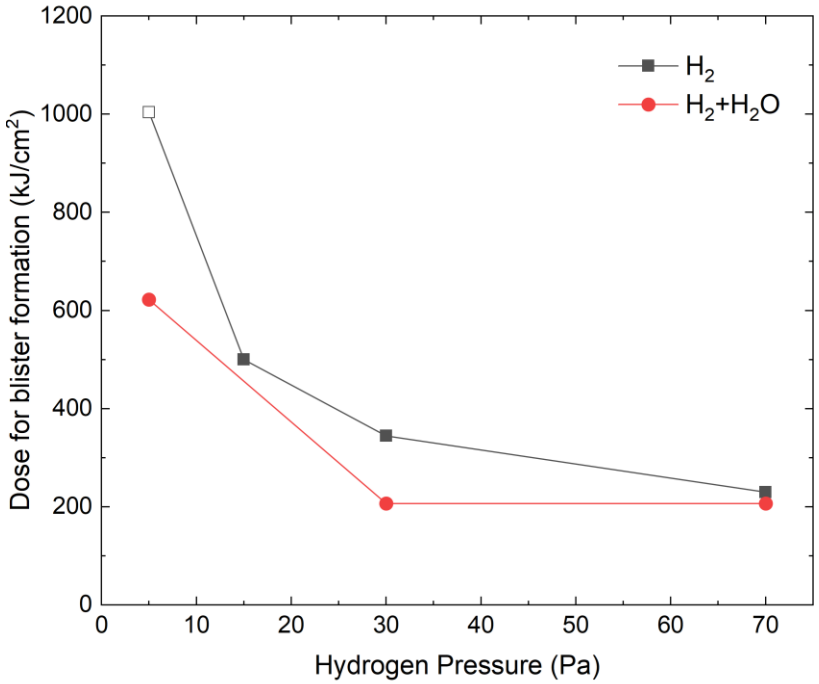

Fig. 4 EUV dose dependence of blister formation on hydrogen pressure and water vapor on the mask blanks #1-4, #6-8. The white dot indicates no blister formed.

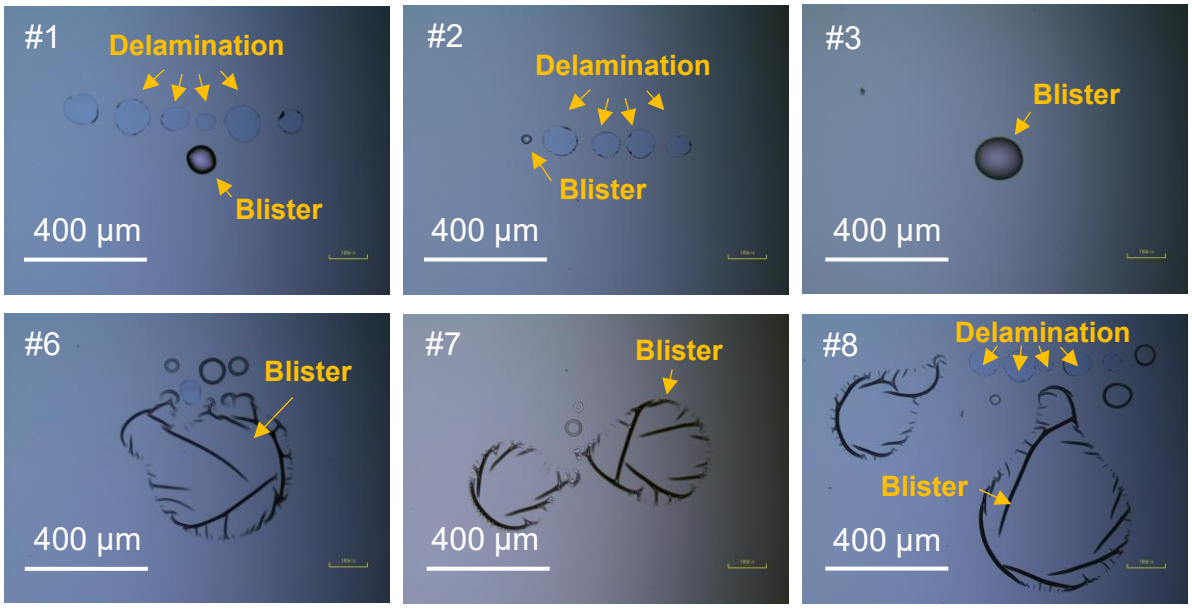

Fig. 5 Microscope images of blister formation on the mask blanks

Fig. 6-(a) shows the scanning electron microscopy (SEM) image of the blisters on the mask blank #6 after the EUV acceleration tests with hydrogen and water vapor at the blister position. Fig. 6-(b) shows the cross-sectional scanning transmission electron microscopy (STEM) image cut along the yellow dashed line of Fig. 6-(a). A delamination was observed at the interface between the Ru capping layer and the top-Si layer of the ML, and no delamination within the ML.

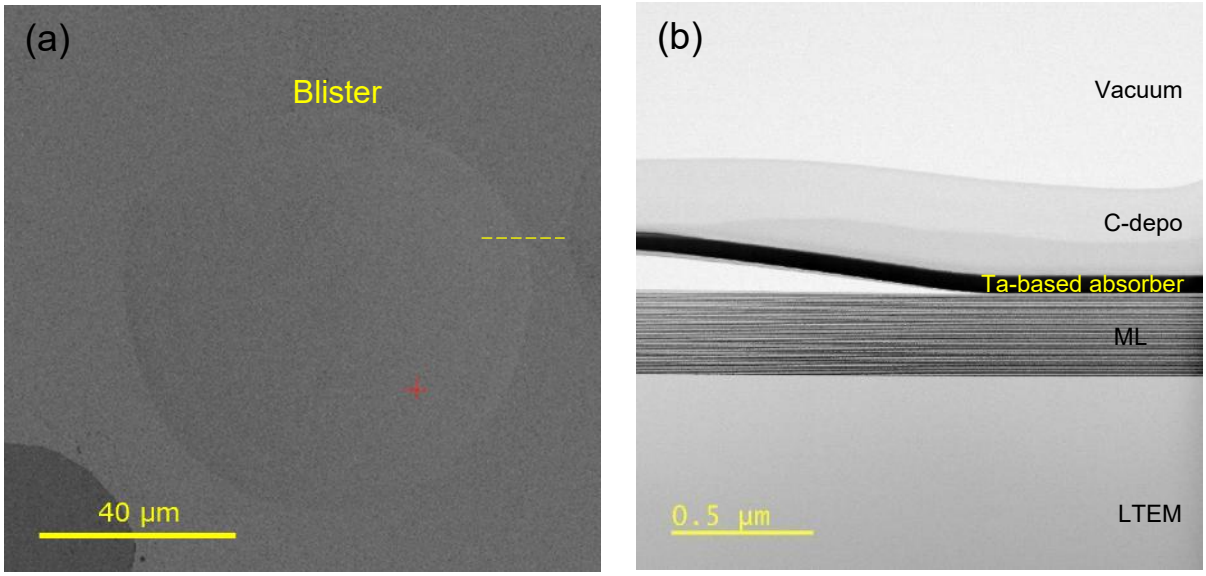

Fig. 6 (a) SEM image of blister on the surface of the mask blank #6 after the EUV irradiation with hydrogen and water vapor at the blister position, (b) Cross-sectional STEM image observed along the yellow dashed line of Fig. 6-(a).

3.2 Photomasks

Table 2 shows the EUV accelerated lifetime test results on the photomask fragments #10 and #11. Both samples were tested under hydrogen at 5 Pa, and water vapor was additionally introduced for #11. Blisters were observed in both samples, with total exposure doses of 178.9 kJ/cm² for #10 (hydrogen only) and 108.6 kJ/cm² for #11 (hydrogen with water vapor). The introduction of water vapor reduced the blister formation dose by 70.3 kJ/cm² (approximately 39%). The water-induced acceleration of blister formation observed in the mask blanks was also reproduced in photomasks fabricated with different materials and processes.

Table 2 Hydrogen and water vapor plasma durability test results on EUV photomasks

No.	Sample	EUV intensity (W/cm^2)	H_2 Pressure (Pa)	H_2O Pressure (Pa)	Blister	Blister formation time (min)	Blister formation dose (kJ/cm^2)
10	Photomask	47.3	5	0	**Observed**	63	178.9
11		39.8	5	10^{-3}	**Observed**	57	108.6

4 Surface analysis

4.1 XAS profile on mask blanks

We measured the EUV reflectivity of 13.5 nm wavelength to identify the irradiated and the unirradiated positions on the mask blanks #2 and #7 as shown in Fig. 7. At the irradiated positions, the increase of approximately 4 % in reflectivity was observed under hydrogen only conditions, whereas under hydrogen with water vapor conditions, the increase of approximately 0.5 % was observed. We measured the surface oxidation using O *K*-edge energy from X-ray absorption spectroscopy (XAS) on #2 and #7. Fig. 8 shows the XAS spectra to compare the oxidation between the unirradiated and irradiated positions. The results show significant differences in the normalized intensity around 543 eV, indicating that oxidation occurred in both the hydrogen-only and the water-vapor cases.

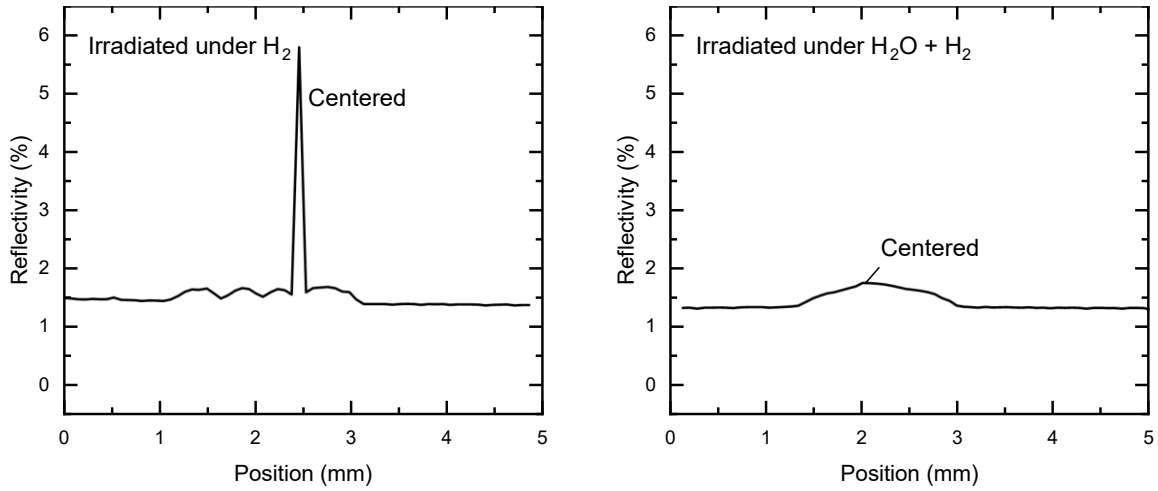

Fig. 7 EUV reflectivity of the irradiated and the unirradiated positions on the mask blanks #2 and #7.

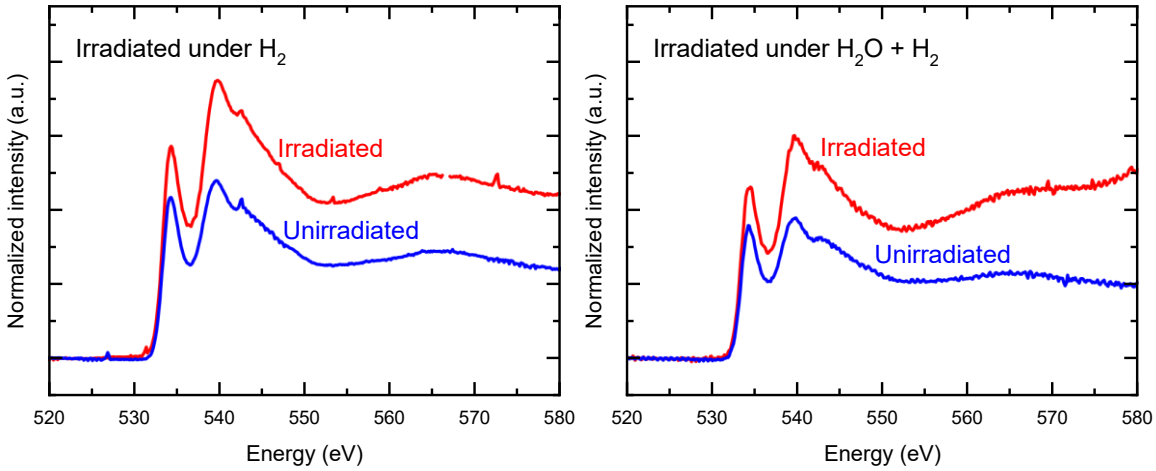

Fig. 8 XAS spectra on the mask blanks #2 and #7 after the EUV irradiation at the blister positions.

4.2 Hydrogen profile on photomasks

Fig. 9 shows the Rutherford backscattering spectrometry (RBS) results for the nanoscale-converted elemental depth profiles of the photomask #11 in the unirradiated and the irradiated positions. In the irradiated profiles, hydrogen was concentrated near the surface at depth of around 0 to 15 nm, accompanied by carbon and minor amounts of oxygen and nitrogen. Below the surface region, Ta-based absorbers were observed with an approximately constant atomic ratio around 0.5 extending to about 60 nm. Around 60 to 75 nm, Ta decreased while Si and Mo increased and reached atomic ratios of 0.6 and 0.4, respectively. After irradiation, the hydrogen signal increased compared with the pre-irradiation profile, showing higher intensity from the surface down to the Mo/Si ML, whereas the signal from the Ru capping layer and the internal interfaces of the ML remained unchanged.

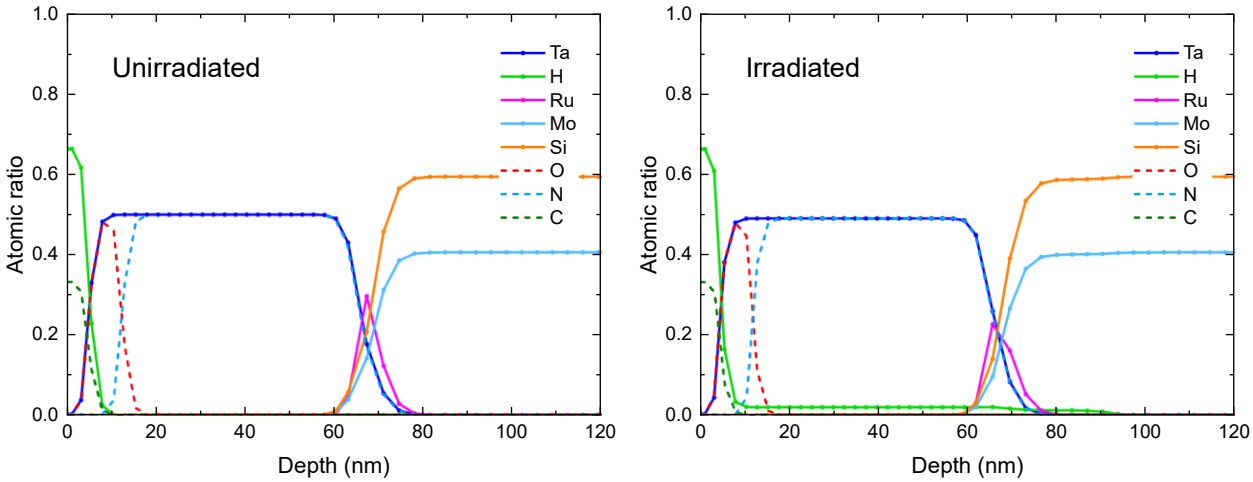

188

189 **Fig. 9** RBS results of the photomask #11 in the unirradiated and the irradiated positions.

190

191 Fig. 10 shows the hydrogen forward scattering spectrometry (HFS) spectra obtained from the
192 unirradiated and irradiated regions of photomask #11. In HFS, hydrogen atoms located at greater
193 depths are detected at lower energies owing to the larger energy loss during scattering. The result
194 indicates that hydrogen near the surface gave rise to the main peak at around 750-800 keV,
195 whereas hydrogen distributed deeper in the structure appeared on the lower-energy side of the
196 spectrum. The irradiated region showed a higher hydrogen yield than the unirradiated region in
197 the 600-740 keV range.

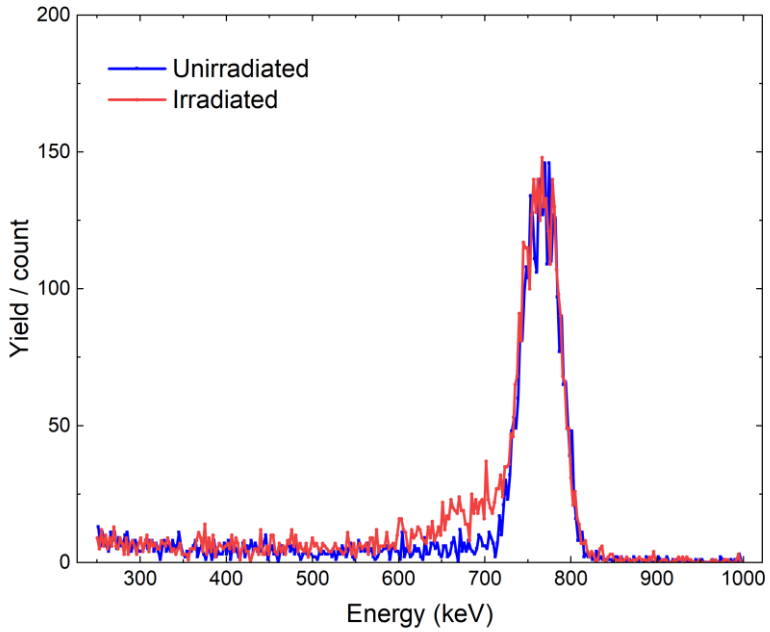

198

199 **Fig. 10** HFS results of the photomask #11 in the unirradiated and the irradiated regions.

5 Conclusion

We investigated blistering on EUV mask blanks under EUV-induced plasma environments with hydrogen and water vapor. We found that blisters formed in shorter times at higher hydrogen pressures in the range of 5 to 70 Pa, and that the introduction of water vapor at 10^{-3} Pa further boosted blister formation at lower hydrogen pressures. STEM observation revealed that the blister occurred at the interface between the Ru capping layer and the top-Si layer of the Mo/Si ML, even under water vapor introduction. XAS, RBS, and HFS results clarified that water vapor enhances surface oxidation and that hydrogen accumulates in near-surface layers during EUV exposure. Our results provide insight into the chemical and physical reactions of nanoscale films on EUV masks and contribute to the development of next-generation mask processes.

Disclosures

The authors declare that there are no financial interests, commercial affiliations, or other potential conflicts of interest that could have influenced the objectivity of this research or the writing of this paper.

Code, Data, and Materials Availability

The data that supports the findings of this study are available from the corresponding authors on request.

Acknowledgments

This work was partially supported by Hyogo Earthquake Memorial 21st Century Research Institute, Hyogo Foundation for Science and Technology, Tanaka Kikinzoku Memorial Foundation, and Takahashi Industrial and Economic Research Foundation.

References

1. J. van Schoot, “Exposure tool development toward advanced EUV lithography: A journey of 40 years driving Moore’s law,” *IEEE Electron Devices Magazine* **2**(1), 8-22 (2024)
2. A. Barty and K. A. Goldberg, "Effects of radiation-induced carbon contamination on the performance of an EUV lithographic optic," *Proc. SPIE* **5037** 450-459 (2003).

3. Y. Nishiyama et al., "Carbon contamination of EUV mask: film characterization, impact on lithographic performance, and cleaning," *Proc. SPIE* **6921**, 338-347 (2008).
4. N. B. Koster et al., "A multistep approach for reticle cleaning," *Proc. SPIE* **8322** 217-227 (2012).
5. A. Dolgov et al., "Comparison of H2 and He carbon cleaning mechanisms in extreme ultraviolet induced and surface wave discharge plasmas," *J. Phys. D: Appl. Phys.* **47**(6), 065205 (2013).
6. J. M. Pommersheim et al., "Prediction of blistering in coating systems," *Organic Coatings for Corrosion Control*, Chap. 11, 137-150 (1998).
7. A. S. Kuznetsov et al., "Blistering behavior in Mo/Si multilayers," *Proc. SPIE* **8077**, 253-260. (2011).
8. T. Hiroaki et al., "Evaluation of hydrogen-induced blistering of Mo/Si multilayers with a capping layer," *Plasma Fusion Res.* **17**, 1406005 (2022).
9. E. S. Choe et al., "Evaluation of H2 Plasma‐Induced Damage in Materials for EUV Lithography," *Adv. Mater. Interfaces* **11**(7), 2300867 (2024).
10. H. Ishida et al., "Development of an EUV irradiation tool in hydrogen atmosphere to evaluate EUV mask absorber durability," *Jpn. J. Appl. Phys.* **64**(3), 03SP71 (2025).
11. R. Klein et al., "Lifetime testing of EUV optics using intense synchrotron radiation at the PTB radiometry laboratory," *Proc. SPIE* **4506**, 105-112 (2001).
12. C. C. Wu et al., "Lifetime test on EUV photomask with EBL2," *Proc. SPIE* **11178**, 94-99 (2019).
13. T. Harada et al., "Development of a high-power EUV irradiation tool in a hydrogen atmosphere," Jpn. *J. Appl. Phys.* **60**(8), 087005 (2021).
14. J. K. Stortelder et al., "First experimental evaluation of accelerated reticle lifetime testing using an applied bias voltage at EBL2," *Proc. SPIE* **13687**, 75-84 (2025).
15. R. Jonckheere et al., "Study of EUV reticle storage effects through exposure on EBL2 and NXE," *Proc. SPIE* **11517**, 78-90 (2020).
16. G. Yetik et al., "Real-time observation of EUV-induced blister formation at various sample temperatures in pellicle-like materials," *Proc. SPIE* **13686**, 206-218 (2025).
17. J. Stortelder et al., "Compatibility assessment of novel reticle absorber materials for use in EUV lithography systems," *Proc. SPIE* **10957**, 259-267 (2019).
18. J. Stortelder et al., "First results of EUV-scanner compatibility tests performed on novel 'high-NA' reticle absorber materials," *Proc. SPIE* **11854**, 103-114 (2021).
19. M. van de Kerkhof et al., "Plasma-assisted discharges and charging in EUV-induced plasma," *J. Micro/Nanopattern. Mater. Metrol.* **20**(1), 013801 (2021).
20. M. van de Kerkhof et al., "EUV-induced hydrogen plasma: pulsed mode operation and confinement in scanner," J. Micro/Nanopattern. Mater. Metrol. **20**(3), 033801 (2021).

21. M. van de Kerkhof et al., "EUV-induced hydrogen plasma and particle release," *Radiat. Eff. Defects Solids* **177**(5-6), 486-512 (2022).
22. K.W. Lu et al., “The effect of hydrogen ion bombardment on the capping layers of extreme ultraviolet mirrors,” *Mater. Res. Express* **12**(4), 046402 (2025).
23. T. E.Madey et al., "Surface phenomena related to mirror degradation in extreme ultraviolet (EUV) lithography," *Appl. Surf. Sci.* **253**(4) 1691-1708 (2006).
24. A. L. Bondareva, G. I. Zmievskaya, "Computer simulation of blistering in multilayer mirrors for EUV lithography," *J. Surf. Investig.: X-ray Synchrotron Neutron Tech.* **4**(3) 480-487 (2010).
25. T. H. M. Van De Ven et al., "Ion energy distributions in highly transient EUV induced plasma in hydrogen," *J. Appl. Phys.* **123**(6) (2018).
26. M. van de Kerkhof, "Interaction between EUV and construction materials," *Proc. SPIE* **13533**, 37-41 (2025).
27. N. Cabrera, N. F. Mott, "Theory of the oxidation of metals," *Rep. Prog. Phys.* **12**(1) 163 (1949).
28. E. A. Gulbransen et al., "Oxidation of Molybdenum 550 to 1700 C," *J. Electrochem. Soc.* **110**(9), 952 (1963).
29. M. R. Louthan Jr et al., "Hydrogen embrittlement of metals," *Mater. Sci. Eng.* **10**, 357-368 (1972).
30. M. van de Kerkhof et al., “High-transmission EUV pellicles supporting > 400W source power,” *Proc. SPIE* **12051**, 70-77 (2022).

Biographies and photographs for the other authors are not available.